AGU ADVANCING EARTH AND SPACE SCIENCE

Geophysical Research Letters

RESEARCH LETTER
10.1029/2020GL090371

Key Points:

- Seismicity rates in Montana and Idaho, excluding Yellowstone, exhibit seasonal signals with most events occurring in winter
- Seismicity rate variations are most strongly correlated with maximum hydrologic loading rate
- Intraplate crust in the northern Rockies is critically stressed

Supporting Information:

- Supporting Information S1

Correspondence to:
M. Perry,
mason.perry@umontana.edu

Citation:
Perry, M., & Bendick, R. (2021). Intraplate seasonal seismicity in the northern Rocky Mountains of Montana and Idaho. *Geophysical Research Letters*, *48*, e2020GL090371. https://doi.org/10.1029/2020GL090371

Received 14 AUG 2020
Accepted 5 JAN 2021

Intraplate Seasonal Seismicity in the Northern Rocky Mountains of Montana and Idaho

M. Perry[1] **and R. Bendick**[1]

[1]Department of Geosciences, University of Montana, Missoula, MT, USA

Abstract Hydrologic processes have been shown to influence seismic productivity in many regions around the world, especially on active plate boundaries. To examine the influence of hydrologic loading cycles on seismicity in intraplate regions, we investigate temporal patterns of seismic productivity in the northern Rocky Mountains of Montana and Idaho. Seasonal variations in seismicity are present, with enhanced productivity in December and January, and reduced productivity in June and July. Using Snowpack Telemetry and GPS data, we find that seismicity is temporally correlated with the highest hydrologic loading rates rather than peak load, consistent with rate and state models of fault behavior for faults in critically stressed domains. However, we cannot distinguish between high hydrologic stress rates and pore pressure increases at seismogenic depths lagging ~6 months after peak snowmelt.

Plain Language Summary Earthquake catalogs from the Rocky Mountains of Montana and Idaho show increased seismicity occurring during December and January. Increased seismic activity is strongly correlated with loading rate from snowfall, though it could alternatively be linked to seasonal changes in regional groundwater hydrology.

1. Introduction

Redistribution of surface mass loads by the hydrosphere has been shown to elicit geodetically measurable elastic deformation of the Earth's surface (e.g., Argus et al., 2014; Birhanu & Bendick, 2015; Borsa et al., 2014; Fu et al., 2015, 2012; Larochelle et al., 2018), perturb the state of stress in the crust, and promote or inhibit seismicity (e.g., Bettinelli et al., 2008; Bollinger et al., 2007; Craig et al., 2017; Heki, 2003; Johnson et al., 2017a, 2017b; Xue et al., 2020). In tectonically active regions, temporal loads associated with positive coulomb stress lead to seismicity rate increases; loads associated with negative coulomb stress lead to decreased seismicity rates, consistent with models in which faults at plate boundaries are usually near failure (i.e., critically stressed). Influxes of meteoric water have also been shown to influence seismicity rate by inducing changes in pore pressure and frictional coefficients at depth (e.g., Wolf et al., 1997). Increases in seismic productivity (i.e., seismicity rate) from pore pressure diffusion have a lag from peak runoff and infiltration as pore pressure diffuses to seismogenic depth (Bollinger et al., 2007; Christiansen et al., 2005; Costain, 2008; Johnson et al., 2020; Montgomery-Brown et al., 2019; Saar & Manga, 2003).

Most studies of seasonal modulation of seismicity consider active plate boundaries where tectonic motions provide steady loading to critically stress the crust (e.g., Johnson et al., 2017a, 2017b), such that small additional stress perturbations suffice to change seismic productivity. Intraplate regions, largely due to their aseismic nature have rarely been subject to similar studies, though Craig et al. (2017) suggest that seasonal loading influences rates of microseismicity in the New Madrid Seismic Zone. While many studies use other observations to imply that intraplate crust is critically stressed (e.g. Townend & Zoback, 2000; Zoback & Townend, 2001; Zoback et al., 2002), in situ stress measurements remain relatively sparse and limited to shallow portions of the crust (Heidbach et al., 2018), precluding full characterization of the of the strength of intraplate continental seismogenic crust.

The northern Rocky Mountains of Montana and Idaho provide an opportunity to investigate if seasonal loads can influence intraplate seismicity, and therefore to consider the state of stress of intraplate crust, where much of the stress is derived from gradients in body forces rather than tectonic boundary forces. The region contains several seismically active features that imply low-strain-rate tectonic loading: the Intermountain Seismic Belt (ISB), the Centennial Tectonic Zone (CTZ), and the Yellowstone Caldera (Figure 1),

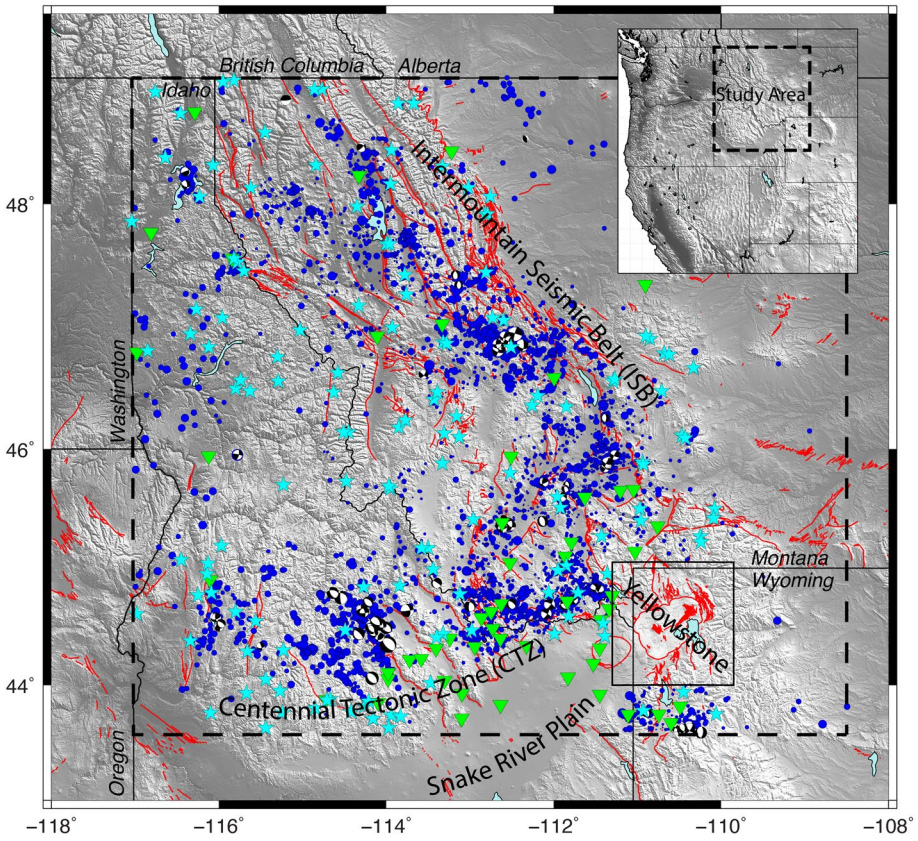

Figure 1. Map of the study area. Important tectonic features are labeled. Mapped faults are plotted in red, seismicity is dark blue circles sized by magnitude. All seismicity in the Yellowstone region has been removed. SNOTEL and GPS stations used in our analysis are plotted as light blue stars and green triangles, respectively. SNOTEL, Snowpack Telemetry; GPS, global positioning system.

all regularly producing small to moderate sized earthquakes (≤M5), punctuated by larger events such as the March 31, 2020 M 6.4 Cascade, Idaho event. Characterized by basin and range style extension and orogenic collapse, the overall state of stress in the region is largely extensional (Faulds & Varga, 1998; Payne et al., 2012, 2013; Schmeelk et al., 2017) with strain accumulation, that is, ~3% that of the nearest plate boundary (Kreemer et al., 2014). Lastly, regional Quaternary deformation is characterized by normal and strike-slip faults (Harkins et al., 2005; Scott et al., 1985; Stickney & Bartholomew, 1987) and resolved focal mechanisms show primarily normal and strike-slip events (Stickney & Bartholomew, 1987), many of which occur on unmapped faults (McMahon et al., 2019; Qamar et al., 1982, Smith et al., 2021) (Figure 1). The region is also host to a large seasonal snowpack that builds from late fall and melts off in late spring to early summer (Serreze et al., 1999). Furthermore, there is good coverage throughout the region in Snowpack Telemetry (SNOTEL) and GPS stations (Figure 1), allowing us to characterize seismicity rate variations in relation to the magnitude and spatial and temporal extent of annual hydrologic loads.

2. Data and Methods

2.1. Earthquake Catalogs, Declustering, and Seismic Analysis

We use hypocenters from the USGS catalog (https://earthquake.usgs.gov/earthquakes/search) for the study region (Figure 1). While the entire ISB extends south to Arizona (R. B. Smith & Sbar, 1974), we only include the ISB north of the Snake River Plain to limit bias from large regional variations in climate and thus hydrologic loading. We also remove all events within a box surrounding the Yellowstone Caldera (Figure 1) to avoid known seasonality of the Yellowstone hydrothermal system (Christiansen et al., 2005). A summary of catalog metadata is shown in Table S1.

The catalog exhibits a temporally variable magnitude of completeness (Figure S1) from January 1975 to January 2020. We therefore separate it into two different catalogs, cat1 from January 2014 to January 2020 with $M_c = 1.1$ and $b = 0.65$, and cat2 from January 1975 to January 2020 with $M_c = 3.0$ and $b = 0.88$. These two different catalogs allow for statistical analyses that better resolve variability in either more complete data sets or longer time series, respectively.

We use the completeness magnitude-independent algorithm developed by Zaliapin and Ben-Zion (2013a, 2013b) to remove aftershock sequences. While several other declustering algorithms were tested (i.e., Gardner & Knopoff, 1974; Reasenberg, 1985), we use the well-characterized July 6, 2017 M5.8 Lincoln, MT event and its aftershock sequence to assess declustering effectiveness. The Zaliapin and Ben-Zion method is most consistent between epochs before and after the test main shock (Figures S1 and S5, Table S2). The declustered cat1 used for analysis contains 3,433 events, while the declustered cat2 contains 670 events. After declustering, both catalogs are further binned into "long-form" and "stacked" catalogs. The long-form catalogs consist of monthly event sums for the catalog duration. The stacked catalogs sum events over all years by month.

2.2. Time Series Analysis and Statistics

To compare variations in seismic productivity with seasonal hydrologic mass loads, we use two independent measures of hydrologic loading: snowpack telemetry (SNOTEL) snow water equivalent (SWE), and vertical GPS displacements. GPS vertical displacements reflect deflection of the crust excited by changes in hydrologic load; SNOTEL SWE measures effective snow depth at specific locations. In the Northern Rockies snowpack is the dominant hydrologic input (Serreze et al., 1999), and the two measures are correlated (Knappe et al., 2019).

Time series of SWE from 1975 to 2020 from 159 SNOTEL stations within our study area (Figure 1, Table S4) were downloaded from the Natural Resources Conservation Service (https://www.wcc.nrcs.usda.gov/snow/). As with the seismic catalog, SNOTEL stations located within the Yellowstone region are omitted. Outliers in the individual time series, defined as observations more than 3 standard deviations away from the best-fit annual sinusoid, are removed and the time series are then smoothed using a 30-day rolling mean. The rate of change in SWE is then found by taking the daily temporal derivative of the smoothed series using centered differencing.

GPS time series from 89 continuously operating stations (Figure 1) were downloaded from the University of Nevada Geodetic Laboratory (Blewitt et al., 2018) in the IGS2014 reference frame (Altamimi et al., 2016). Stations with large data gaps (>2 years), those that ran for fewer than 2 years between 2014 and 2020, and those near Yellowstone were omitted, leading to a total of 57 stations used in our analysis (Table S5). To isolate hydrologic loads, nontidal atmospheric loading was removed using models from the Earth Systems Modeling Group at GFZ (Dill & Dobslaw, 2013). Outliers, defined as measurements greater than 3 standard deviations from the best-fit annual sinusoid were removed and then the time series were detrended and smoothed using a 30-day rolling mean. The temporal derivative of the smoothed GPS time series is also taken daily using centered differencing to compare seismicity with the geodetically derived loading rate.

We use Schuster spectra to look for periodicity in the declustered earthquake catalogs (Ader & Avouac, 2013). An extension of the Schuster test (Schuster, 1897), Schuster spectra test if a catalog contains one or more interevent intervals that are more common than expected by comparing all the natural interevent intervals to a random walk distribution (Ader & Avouac, 2013). The Schuster p-value is therefore the likelihood that apparent temporal patterns are due to chance (Schuster, 1897). To verify these bootstrapped probabilities, we also compare the difference in the number of winter and summer events in our natural catalog with that of 10,000 randomly generated (Monte Carlo) catalogs of the same magnitude-frequency distribution. Following Christiansen et al. (2005), we finally perform a Kruskal-Wallis test on the binned catalogs (Kruskal & Wallis, 1952), as a way to determine if different subsets of events (i.e., events in winter vs. events in summer), assumed to be independent, are likely from the same initial distribution.

Next, we compare observed seismicity rate variations with the regionally averaged time series of all GPS and SNOTEL stations in the study area (i.e., the common mode), and their temporal derivatives, representing time series of the regional-scale hydrologic load and loading rate. These time series and derivatives are

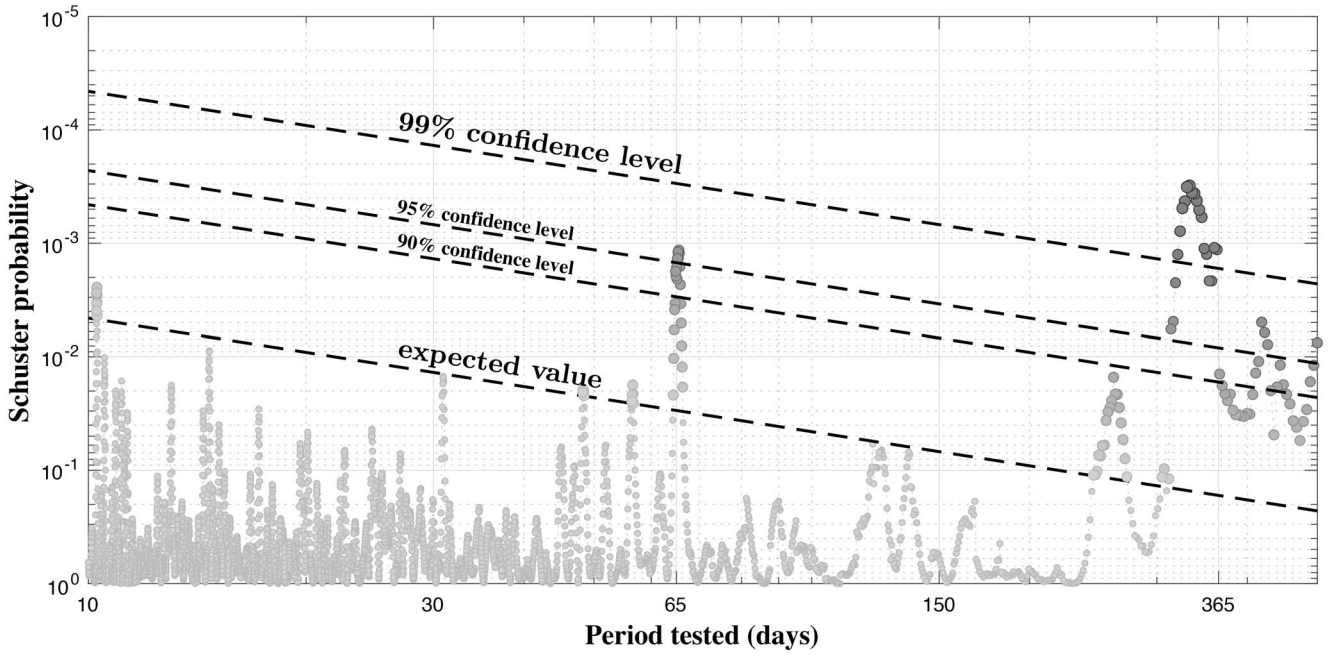

Figure 2. Schuster spectrum of cat1 (2014–2020). Peak exists ~330 days and above the 99% confidence interval.

binned and averaged monthly into long-form and stacked versions to allow for direct comparison to the corresponding earthquake catalogs. We use Pearson's correlations to compare all the time series, common modes, and individual GPS and SNOTEL time series, with the earthquake catalogs. Lastly, we use cross correlations with the earthquake catalogs and common mode time series to investigate any potential time lags between our measures of regional hydrologic loading and seismic productivity.

3. Results

We find evidence to support seasonally modulated seismicity rates in cat1 (Figure 2), but not in cat2 (Figure S2a). In cat1 (2014–2020), the Schuster spectrum shows a statistically significant peak (>99% confidence) at a ~1-year interval (Figure 2). Additional statistical tests on cat1, including the Monte Carlo and Kruskal-Wallis tests indicate that elevated seismicity levels in the winter (Dec and Jan), compared to seismicity levels in the summer (Jun and Jul) are statistically unlikely to be from the same distribution ($P < 0.01$) (Table S3).

Maximum seismic productivity occurs in the winter, and minimum seismic productivity in the summer in cat1 (Figures 3 and S3). These patterns are not strongly correlated with the magnitude of regionally averaged SNOTEL SWE and GPS displacement in either the long form ($R < 0.3$) or stacked ($R < 0.4$) cat1, but there is a stronger correlation and anticorrelation with the rate of change (first derivatives) of SNOTEL SWE ($R = 0.63$) and vertical GPS displacement ($R = -0.69$) stacked time series (Table 1). These are expected to be opposite as increased snow load (a positive change) deflects the crust (a negative change). Similarly, the stacked and binned cat2 (1975–2020), despite limited statistical support for seasonality, shows the strongest correlation with the stacked SNOTEL SWE-derived rate at $R = 0.55$.

Cross correlation of cat1 (2014–2020) with SWE and GPS show seismic productivity most closely matching the common mode SWE rate and common mode GPS rate in both the long form and the stacked versions (Figures 4a and 4b).

Cross correlation with the stacked cat2 (1975–2020) with SWE and GPS show common mode SWE rate is most closely correlated with seismic productivity (Figure 4c). Cross correlations of the long form time series with common mode SWE and SWE rate have low magnitudes with little change across the tested phase shifts.

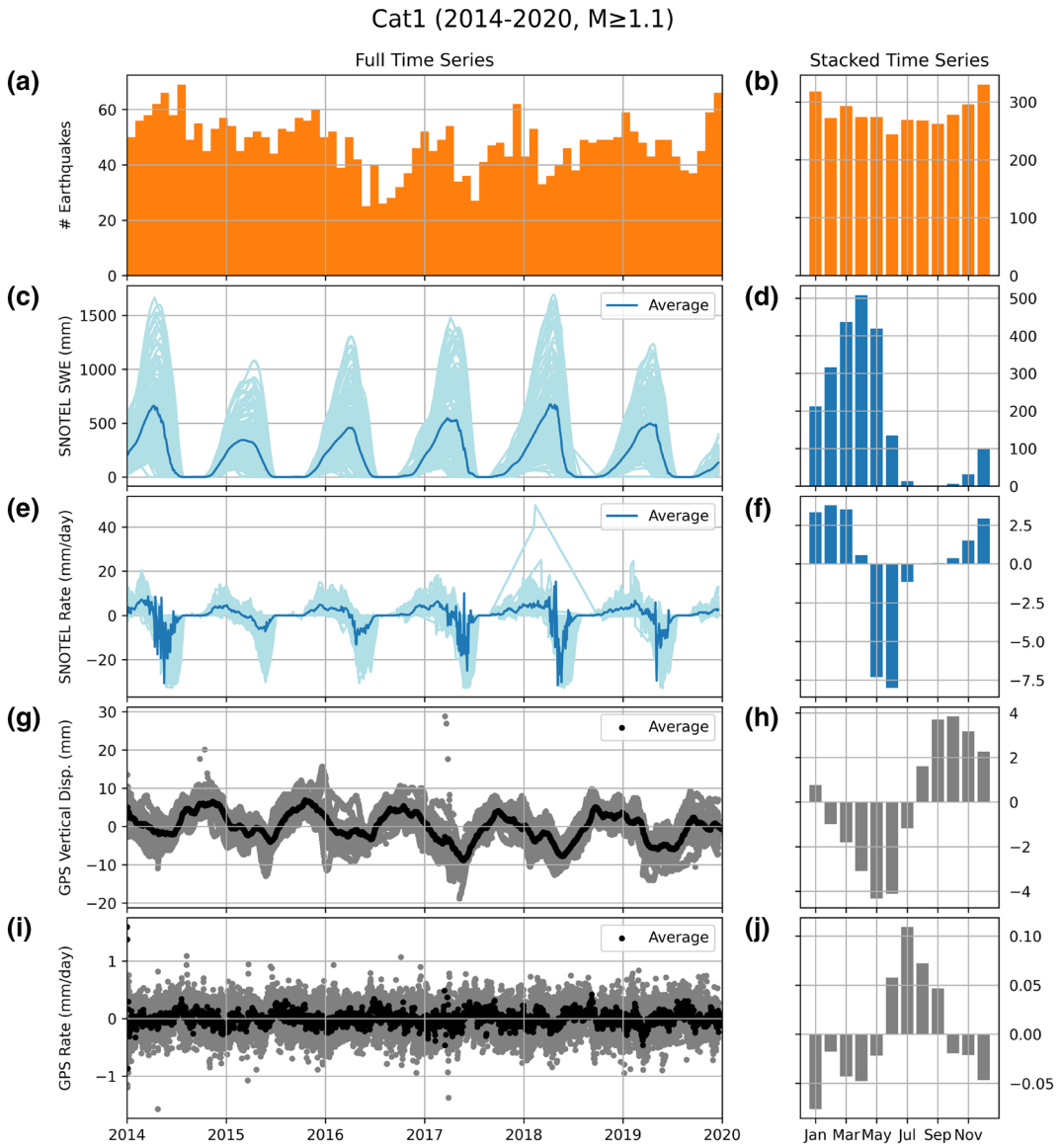

Figure 3. Comparison of earthquake catalogs to SNOTEL and GPS time series. The left column (a, c, e, g, i) shows full time series while the right column (b, d, f, h, j) shows stacked time series with total events for the earthquake catalog, and averaged measurements for SNOTEL and GPS. Units are the same across rows. (2a) shows the full earthquake catalog in monthly bins. (2c) shows SNOTEL SWE time series in mm, with smoothed time series for each stain in light blue, and the averaged regional SWE in dark blue. (2e) shows the SNOTEL-SWE derived rate in mm/day with the same color scheme as (2c). (2g) shows the detrended and smoothed vertical GPS time series in mm, with each station plotted in gray, and the regional average in black. (2i) shows the vertical GPS-derived rate in mm/day with the same color scheme as (2g). GPS, global positioning system; SNOTEL, snowpack telemetry; SWE, snow water equivalent.

4. Discussion

There is evidence of seasonal seismicity in the northern Rocky Mountains, with modest, but measurable peaks in seismic productivity during December and January. Similar to results found by Craig et al. (2017), this seasonality is largely limited to small magnitude events, as seasonality disappears in cat2 (M_c = 3.0) though this may be an artifact of the limited catalog duration, hence the paucity of larger recorded events in the study region.

Table 1
Summary of Pearson's correlations

	SNOTEL SWE	SNOTEL SWE rate of change	GPS	GPS rate of change
Cat1 – Full	0.04	0.22	0.26	−0.11
Cat1 – Stacked	0.05	0.63	0.37	−0.69
Cat2 – Full	0.03	0.11	N/A	N/A
Cat2 – Stacked	0.21	0.55	N/A	N/A

Abbreviations: GPS, global positioning system; SNOTEL, Snowpack Telemetry; SWE, snow water equivalent.

Increased seismic productivity is coincident with peaks in vertical loading rate inferred from GPS and SNOTEL SWE (Figures 3 and 4). This is similar to the relationship observed in the Himalaya (Ader et al, 2014; Bettinelli et al., 2008) and on dip-slip faults in California (Johnson et al., 2017a), despite the fundamental differences in tectonic setting. However, the amplitudes of the response differ, with Himalayan seismic productivity varying by 40% seasonally, productivity in the study area varying by 20%, and in California by ∼15%. Based on models of harmonic stress perturbations on rate and state faults by Ader et al. (2014), this difference in productivity amplitude implies that the nucleation time for events in the North American interior is longer than that in the Himalaya and shorter than for dip-slip faults in California. The rate-and-state formulation also offers an explanation for the observed magnitude bias in correlation with loading rate, because the larger events in cat2 would be expected to have a characteristic nucleation time much longer than the period of seasonal loading, leading to complete damping of the annual periodic contribution. Only the smallest events in the regional catalog have sufficiently short nucleation times to couple to the periodic seasonal loading rate change.

In addition to an amplitude relationship to the period of harmonic stress changes, fault response to harmonic perturbations also has a phase relation, such that if the stress function has a period less than the critical nucleation period, the seismic productivity is in phase with the stress perturbation as observed in the New Madrid seismic zone (Craig et al., 2017). If the stress function has a period greater than the nucleation period, the productivity is in phase with the rate of shear-stress perturbation. The observed phase shift between the maximum normal loading from hydrologic mass loads and the seismic productivity in our study area is, as with the amplitude argument above, consistent with a nucleation period of less than one year for the fault segments in the study area, whereas faults in New Madrid have significantly longer nucleation periods (>8–10 years) (Craig et al., 2017).

Assuming uniaxial vertical stress (i.e. $\varepsilon_v E = \sigma_v$; E = 70 GPa; h_{crust} = 45 km), we estimate a maximum vertical stress perturbation near the surface on the order of ∼16 kPa over the course of a year associated with seasonal loading, derived from peak-to-trough change in vertical position of ∼10.6 mm in the common mode time series. Values calculated for each GPS station range from ∼12–33 kPa associated with average peak-to-trough displacements of ∼8–21 mm (Table S5). This considerably exceeds estimates of stresses as low as 2–5 kPa entraining seismic productivity in the western U.S. (e.g. Christiansen et al., 2005; Christiansen et al., 2007) or 2–4 kPa in the Himalaya (Bollinger et al., 2007). Although the surface mass loading produces stresses with larger magnitudes than other study locations, the magnitude of seasonal stress changes is still small, on the order of kPa, so the presence of temporally variable seismicity requires large background static stresses. Regional deformation in the Rockies, far from the plate boundary to the west, is dominated by extensional deviatoric stresses linked to gravitational potential energy (GPE), rather than tectonic boundary conditions (Flesch et al., 2000, 2007). Thus, σ_1, the largest principal background stress, is oriented vertically or near vertically throughout much of the study region, (Flesch et al., 2007; Schmeelk et al., 2017). The principal stress orientations from surface mass loading are therefore aligned to the regional stress tensor. We interpret the amplitude and phase of seismic productivity variations along with the stress orientations to indicate that faults in the Intermountain Seismic Zone are always near failure, with characteristic nucleation times similar to faults within active tectonic boundary zones, and thus critically stressed from gradients in body forces. The broader implication of this finding is that crustal faults can be activated by either tectonic boundary forces or gravitational body forces, providing a mechanism for intraplate deformation far from active plate boundaries.

Alternatively, other studies have linked seasonal variations in seismicity to increases in pore pressure with some delay from peak hydrologic load or precipitation (Christiansen et al., 2005; Johnson et al., 2020; Saar & Manga, 2003; Wolf et al., 1997). Invoking this mechanism, seismic productivity increases will occur after a lag from peak runoff and infiltration, which occurs in late spring to early summer (e.g., Knappe et al., 2019) (Figure 3). As this would result in a minimum cross correlation (or maximum anticorrelation) with SWE rate and a maximum cross correlation with GPS rate at a ∼6-month shift, this interpretation is also supported

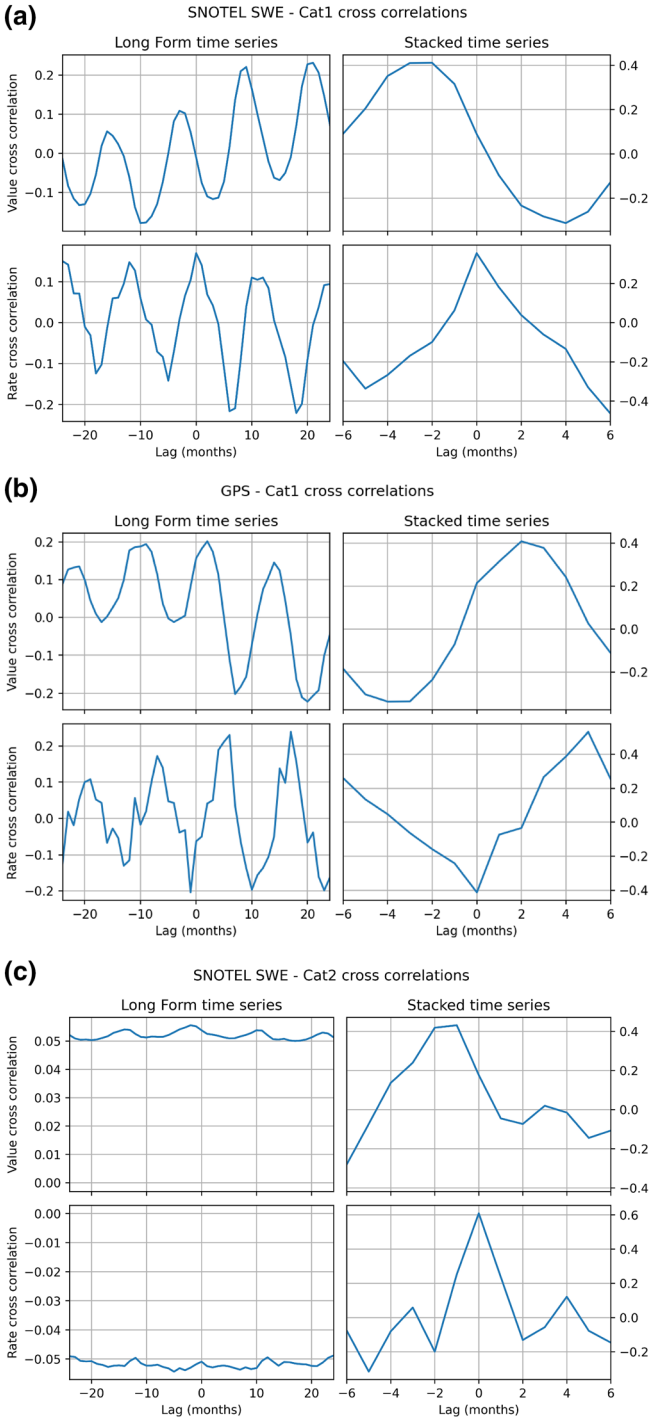

Figure 4. Cross correlations of time series and seismicity rate. (4a) is cross correlations between cat1, SNOTEL SWE, and SWE-derived rate. (4b) is cross correlations among cat1, GPS vertical position, and GPS-derived rate. (4b) is the cross correlations between cat2, SNOTEL SWE, and SWE-derived rate. GPS, global positioning system; SNOTEL, Snowpack Telemetry.

by our analysis (Figure 4). It does however, necessitate high enough crustal permeability for pore pressure diffusion to reach seismogenic depth (5–10 km) in ~6 months. Following Saar and Manga (2003), migration of a pore pressure front to the mean seismogenic depth (8.26 km), requires a bulk hydraulic diffusivity of ~0.69 m^2/s, within the range of hydraulic diffusivities calculated by other studies (Bollinger et al., 2007; Christiansen et al., 2005; Costain, 2008; Saar & Manga, 2003). Furthermore, such regional values are reasonable considering increased fluid flow and hydraulic diffusivity along fault planes and highly fractured regions of the crust (e.g., Stober & Bucher, 2015; Townend & Zoback, 2000; Zoback & Townend, 2001).

While both mechanisms are supported by our observations, we prefer seismic entrainment by dynamic stress increases linked to seasonal loading on critically stressed rate-and-state finite faults, as it avoids making large assumptions about hydraulic properties of a large and geologically heterogeneous region.

5. Conclusions

We find significant evidence for seasonal variations in seismic productivity in the Rocky Mountains of Montana and Idaho. A declustered seismic catalog from 2014 to 2020 shows maximum seismic productivity in the early winter (December and January) and minimum seismic productivity in early summer (June and July), coincident with peaks in loading rate inferred from regional GPS vertical time series, as well as SNOTEL SWE. We attribute the peaks in seismicity to seasonal increases in stress on regional faults whose behavior can be explained under rate and state assumptions (i.e., Ader et al., 2014) within a fault-filled region whose state of stress is dominated by GPE. However, we cannot rule out elevated seismic productivity induced by pore pressure diffusion to seismogenic depth (e.g. Christiansen et al., 2005; Johnson et al., 2020; Saar & Manga, 2003; Wolf et al., 1997), with seismicity following peak runoff and infiltration after a ~6-month lag time.

Regardless of the mechanism(s), the peak in seismic productivity strongly correlated with hydrologic cycles demonstrates that intraplate crust in the Northern Rockies hosts seismogenic fault patches with short characteristic nucleation times; these fail when subject to relatively small stress perturbations at annual periods, and thus can be approximated as critically stressed.

Data Availability Statement

UNAVCO's Plate Boundary Observatory and Idaho National Laboratory for collected and made GPS observations publicly available on the UNAVCO archive (http://www.unavco.org/data/gps-gnss/data-access-methods/dai2/app/dai2.html), the processing group at the Nevada Geodetic Laboratory, which provided publicly available processed GPS data (http://geodesy.unr.edu/links.php).

Acknowledgments
The authors acknowledge UNAVCO's Plate Boundary Observatory and Idaho National Laboratory for collecting and making GPS observations publicly available on the UNAVCO archive (http://www.unavco.org/data/gps-gnss/data-access-methods/dai2/app/dai2.html), as well as the processing group at the Nevada Geodetic Laboratory, which provide publicly available processed GPS data (http://geodesy.unr.edu/links.php). They also acknowledge Christopher W Johnson and an anonymous reviewer for incredibly helpful comments and suggestions. Maps were made using Generic Mapping Tools (GMT) (Wessel et al., 2013).

References

Ader, T. J., & Avouac, J. P. (2013). Detecting periodicities and declustering in earthquake catalogs using the Schuster spectrum, application to Himalayan seismicity. *Earth and Planetary Science Letters*, *377–378*, 97–105. https://doi.org/10.1016/j.epsl.2013.06.032

Ader, T. J., Lapusta, N., Avouac, J. P., & Ampuero, J. P. (2014). Response of rate-and-state seismogenic faults to harmonic shear-stress perturbations. *Geophysical Journal International*, *198*(1), 385–413. https://doi.org/10.1093/gji/ggu144

Altamimi, Z., Rebischung, P., Métivier, L., & Collilieux, X. (2016). ITRF2014: A new release of the international terrestrial reference frame modeling nonlinear station motions. *Journal of Geophysical Research: Solid Earth*, *121*(8), 6109–6131. https://doi.org/10.1002/2016JB013098

Argus, D. F., Fu, Y., & Landerer, F. W. (2014). Seasonal variation in total water storage in California inferred from GPS observations of vertical land motion. *Geophysical Research Letters*, *41*(6), 6413–6419. https://doi.org/10.1002/2014GL059570

Bettinelli, P., Avouac, J. P., Flouzat, M., Bollinger, L., Ramillien, G., Rajaure, S., & Sapkota, S. (2008). Seasonal variations of seismicity and geodetic strain in the Himalaya induced by surface hydrology. *Earth and Planetary Science Letters*, *266*(3–4), 332–344. https://doi.org/10.1016/j.epsl.2007.11.021

Birhanu, Y., & Bendick, R. (2015). Monsoonal loading in Ethiopia and Eritrea from vertical GPS displacement time series. *Journal of Geophysical Research: Solid Earth*, *120*(10), 7231–7238. https://doi.org/10.1002/2015JB012072.Received

Blewitt, G., Hammond, W. C., & Kreemer, C. (2018). Harnessing the GPS data explosion for interdisciplinary science. *EOS*, *99*, 1–2. https://doi.org/10.1029/2018EO104623

Bollinger, L., Perrier, F., Avouac, J. P., Sapkota, S., Gautam, U., & Tiwari, D. R. (2007). Seasonal modulation of seismicity in the Himalaya of Nepal. *Geophysical Research Letters*, *34*(8), 1–5. https://doi.org/10.1029/2006GL029192

Borsa, A. A., Agnew, D. C., & Cayan, D. R. (2014). Ongoing drought-induced uplift in the western United States. *Science*, *345*(6204), 1587–1590. https://doi.org/10.1126/science.1260279

Christiansen, L. B., Hurwitz, S., Saar, M. O., Ingebritsen, S. E., & Hsieh, P. A. (2005). Seasonal seismicity at western United States volcanic centers. *Earth and Planetary Science Letters*, *240*(2), 307–321. https://doi.org/10.1016/j.epsl.2005.09.012

Costain, J. K. (2008). Intraplate seismicity, hydroseismicity, and predictions in hindsight. *Seismological Research Letters*, *79*(4), 578–589. https://doi.org/10.1785/gssrl.79.4.578

Craig, T. J., Chanard, K., & Calais, E. (2017). Hydrologically-driven crustal stresses and seismicity in the New Madrid seismic zone. *Nature Communications*, *8*(1), 2143. https://doi.org/10.1038/s41467-017-01696-w

Dill, R., & Dobslaw, H. (2013). Numerical simulations of global-scale high-resolution hydrological crustal deformations. *Journal of Geophysical Research*, *118*(9), 5008–5017. https://doi.org/10.1002/jgrb.50353

Faulds, J. E., & Varga, R. J. (1998). *The role of accommodation zones and transfer zones in the regional segmentation of extended terranes* (pp. 1–45). Geological Society of America. https://doi.org/10.1130/0-8137-2323-X.1

Flesch, L. M., Holt, W. E., Haines, A. J., & Shen-Tu, B. (2000). Dynamics of the Pacific-North American plate boundary in the western United States. *Science*, *287*(5454), 834–836. https://doi.org/10.1126/science.287.5454.834

Flesch, L. M., Holt, W. E., Haines, A. J., Wen, L., & Shen-Tu, B. (2007). The dynamics of western North America: Stress magnitudes and the relative role of gravitational potential energy, plate interaction at the boundary and basal tractions. *Geophysical Journal International*, *169*(3), 866–896. https://doi.org/10.1111/j.1365-246X.2007.03274.x

Fu, Y., Argus, D. F., & Landerer, F. W. (2015). GPS as an independent measurement to estimate terrestrial water storage variations in Washington and Oregon. *Journal of Geophysical Research: Solid Earth*, *120*(1), 552–566. https://doi.org/10.1002/2014JB011415

Fu, Y., Freymueller, J. T., & Jensen, T. (2012). Seasonal hydrological loading in southern Alaska observed by GPS and GRACE. *Geophysical Research Letters*, *39*(15), 1–5. https://doi.org/10.1029/2012GL052453

Gardner, J. K., & Knopoff, L. (1974). Is the sequence of earthquakes in Southern California, with aftershocks removed, Poissonian? *Bulletin of the Seismological Society of America*, *64*(5), 1363–1367.

Harkins, N. W., Anastasio, D. J., & Pazzaglia, F. J. (2005). Tectonic geomorphology of the Red Rock fault, insights into segmentation and landscape evolution of a developing range front normal fault. *Journal of Structural Geology*, *27*(11), 1925–1939. https://doi.org/10.1016/j.jsg.2005.07.005

Heidbach, O., Rajabi, M., Cui, X., Fuchs, K., Müller, B., Reinecker, J., et al. (2018). The World Stress Map database release 2016: Crustal stress pattern across scales. *Tectonophysics*, *744*, 484–498. https://doi.org/10.1016/j.tecto.2018.07.007

Heki, K. (2003). Snow load and seasonal variation of earthquake occurrence in Japan. *Earth and Planetary Science Letters*, *207*(1–4), 159–164. https://doi.org/10.1016/S0012-821X(02)01148-2

Johnson, C. W., Fu, Y., & Bürgmann, R. (2017). Seasonal water storage, stress modulation, and California seismicity. *Science*, *356*(6343), 1161–1164. https://doi.org/10.1126/science.aak9547

Johnson, C. W., Fu, Y., & Bürgmann, R. (2017). Stress models of the annual hydrospheric, atmospheric, thermal, and tidal loading cycles on California Faults: Perturbation of background stress and changes in seismicity. *Journal of Geophysical Research: Solid Earth*, *122*(12), 10605–10625. https://doi.org/10.1002/2017JB014778

Johnson, C. W., Fu, Y., & Bürgmann, R. (2020). Hydrospheric modulation of stress and seismicity on shallow faults in southern Alaska. *Earth and Planetary Science Letters*, *530*, 115904. https://doi.org/10.1016/j.epsl.2019.115904

Knappe, E., Bendick, R., Martens, H. R., Argus, D. F., & Gardner, W. P. (2019). Downscaling vertical GPS observations to derive watershed-scale hydrologic loading in the Northern Rockies. *Water Resources Research*, *55*(1), 391–401. https://doi.org/10.1029/2018WR023289

Kreemer, C., Blewitt, G., & Klien, E. C. (2014). A geodetic plate motion and global strain rate model. *Geochemistry, Geophysics, Geosystems*. *15*(10), 3849–3889. https://doi.org/10.1002/2014GC005407

Kruskal, W. H., & Wallis, W. A. (1952). Use of ranks in one-criterion variance analysis. *Journal of the American Statistical Association*, *47*(260), 583–621. https://doi.org/10.1080/01621459.1952.10483441

Larochelle, S., Gualandi, A., Chanard, K., & Avouac, J. P. (2018). Identification and Extraction of Seasonal Geodetic Signals Due to Surface Load Variations. *Journal of Geophysical Research: Solid Earth*, *123*(12), 11031–11047. https://doi.org/10.1029/2018JB016607

McMahon, N. D., Aster, R. C., Yeck, W. L., Benz, H. M., Stickney, M. C., & Martens, H. R. (2019). Spatiotemporal analysis of the foreshock–mainshock–aftershock sequence of the 6 July 2017 M w 5.8 Lincoln, Montana, earthquake. *Seismological Research Letters*, *90*(1), 131–139. https://doi.org/10.1785/0220180180

Montgomery-Brown, E. K., Shelly, D. R., & Hsieh, P. A. (2019). Snowmelt-Triggered Earthquake Swarms at the Margin of Long Valley Caldera, California. *Geophysical Research Letters*, *46*(7), 3698–3705. https://doi.org/10.1029/2019GL082254

Payne, S. J., McCaffrey, R., & Kattenhorn, S. A. (2013). Extension-driven right-lateral shear in the centennial shear zone adjacent to the eastern snake river plain, Idaho. *Lithosphere*, *5*(4), 407–419. https://doi.org/10.1130/L200.1

Payne, S. J., McCaffrey, R., King, R. W., & Kattenhorn, S. A. (2012). A new interpretation of deformation rates in the Snake River Plain and adjacent basin and range regions based on GPS measurements. *Geophysical Journal International*, *189*(1), 101–122. https://doi.org/10.1111/j.1365-246X.2012.05370.x

Qamar, A., Kogan, J., & Stickney, M. C. (1982). Tectonics and recent seismicity near Flathead lake, Montana. *Bulletin of the Seismological Society of America*, *72*(5), 1591–1599.

Reasenberg, P. (1985). Second-order moment of central California seismicity, 1969-1982. *Journal of Geophysical Research*, *90*(B7), 5479–5495. https://doi.org/10.1029/jb090ib07p05479

Saar, M. O., & Manga, M. (2003). Seismicity induced by seasonal groundwater recharge at Mt. Hood, Oregon. *Earth and Planetary Science Letters*, *214*(3–4), 605–618. https://doi.org/10.1016/S0012-821X(03)00418-7

Schmeelk, D., Bendick, R., Stickney, M., & Bomberger, C. (2017). Kinematic evidence for the effect of changing plate boundary conditions on the tectonics of the northern U.S. Rockies. *Tectonics*, *36*(6), 1090–1102. https://doi.org/10.1002/2016TC004427

Schuster, A. (1897). On lunar and solar periodicities of earthquakes. *Proceedings of the Royal Society of London*, *61*(369–377), 455–465. https://doi.org/10.1038/056321a0

Scott, W. E., Pierce, K. L., & Hait, M. H. J. (1985). Quaternary tectonic setting of the 1983 Borah Peak earthquake, central Idaho. *Bulletin of the Seismological Society of America*, *75*(4), 1053–1066. Retrieved from http://www.bssaonline.org/content/75/4/1053.short

Serreze, M. C., Clark, M. P., Armstrong, R. L., McGinnis, D. A., & Pulwarty, R. S. (1999). Characteristics of the western United States snowpack from snowpack telemetry (SNOTEL) data. *Water Resources Research*, *35*(7), 2145–2160. https://doi.org/10.1029/1999WR900090

Smith, E. M., Martens, H. R., & Stickney, M. C. (2021). Microseismic evidence for bookshelf faulting in western montana. *Seismological Research Letters*, http://dx.doi.org/10.1785/0220200321

Smith, R. B., & Sbar, M. L. (1974). Contemporary tectonics and seismicity of the Western United States with emphasis on the intermountain seismic belt. *Bulletin of the Geological Society of America*, *85*(8), 1205–1218. https://doi.org/10.1130/0016-7606(1974)85<1205:CTASOT>2.0.CO;2

Stickney, M. C., & Bartholomew, M. J. (1987). Seismicity and Late Quaternary Faulting of the Northern Basin and Range Province, Montana and Idaho. *Bulletin of the Geological Society of America*, *77*(5), 1602–1625.

Stober, I., & Bucher, K. (2015). Hydraulic conductivity of fractured upper crust: Insights from hydraulic tests in boreholes and fluid-rock interaction in crystalline basement rocks. *Geofluids*, *15*(1–2), 161–178. https://doi.org/10.1111/gfl.12104

Townend, J., & Zoback, M. D. (2000). How faulting keeps the crust strong. *Geology*, *28*(5), 399–402. https://doi.org/10.1130/0091-7613(2000)28<399:HFKTCS>2.0.CO;2

Wessel, P., Smith, W. H. F., Scharroo, R., Luis, J., & Wobbe, F. (2013). Generic Mapping Tools: Improved Version Released. *EOS Trans. AGU*, *94*(45), 409–410. https://doi.org/doi:10.1002/2013EO450001

Wolf, L. W., Rowe, C. A., & Horner, R. B. (1997). Periodic seismicity near Mt. Ogden on the Alaska-British Columbia border: A case for hydrologically triggered earthquakes? *Bulletin of the Seismological Society of America*, *87*(6), 1473–1483.

Xue, L., Johnson, C. W., Fu, Y., & Bürgmann, R. (2020). Seasonal seismicity in the Western Branch of the East African Rift System. *Geophysical Research Letters*, *47*(6), 1–9. https://doi.org/10.1029/2019GL085882

Zaliapin, I., & Ben-zion, Y. (2013). Earthquake clusters in southern California I: Identification and stability. *Journal of Geophysical Research*, *118*(6), 2847–2864. https://doi.org/10.1002/jgrb.50179

Zaliapin, I., & Ben-zion, Y. (2013). Earthquake clusters in southern California II : Classification and relation to physical properties of the crust. *Journal of Geophysical Research*, *118*(6), 2865–2877. https://doi.org/10.1002/jgrb.50178

Zoback, M. D., & Townend, J. (2001). Implications of hydrostatic pore pressures and high crustal strength for the deformation of intraplate lithosphere. *Tectonophysics*, *336*(1–4), 19–30. https://doi.org/10.1016/S0040-1951(01)00091-9

Zoback, M. D., Townend, J., & Grollimund, B. (2002). Steady-state failure equilibrium and deformation of intraplate lithosphere. *International Geology Review*, *44*(5), 383–401. https://doi.org/10.2747/0020-6814.44.5.383